

VERY SMALL-SCALE CLUSTERING AND MERGER RATE OF LUMINOUS RED GALAXIES

Morad Masjedi^{1,2}, David W. Hogg¹, Richard J. Cool³, Daniel J. Eisenstein³,
Michael R. Blanton¹, Idit Zehavi^{3,4}, Andreas A. Berlind¹, Eric F. Bell⁵,
Donald P. Schneider⁶, Michael S. Warren⁷, Jon Brinkmann⁸

ABSTRACT

We present the small-scale ($0.01 < r < 8 h^{-1}$ Mpc) projected correlation function $w_p(r_p)$ and real space correlation function $\xi(r)$ of 24520 luminous early-type galaxies from the Sloan Digital Sky Survey Luminous Red Galaxy (LRG) sample ($0.16 < z < 0.36$). “Fiber collision” incompleteness of the SDSS spectroscopic sample at scales smaller than 55 arcsec prevents measurements of the correlation function for LRGs on scales smaller than ~ 0.3 Mpc by the usual methods. In this work, we cross-correlate the spectroscopic sample with the imaging sample, with a weighting scheme to account for the collisions, extensively tested against mock catalogs. We correct for photometric biases in the SDSS imaging of close galaxy pairs. We find that the correlation function $\xi(r)$ is surprisingly close to a r^{-2} power law over more than 4 orders of magnitude in separation r . This result is too steep at small scales to be explained in current versions of the halo model for galaxy clustering. We infer an LRG-LRG merger rate of $\lesssim 0.6 \text{ Gyr}^{-1} \text{ Gpc}^{-3}$ for this sample. This result suggests that the LRG-LRG mergers are not the main mode of mass growth for LRGs at $z < 0.36$.

¹ Center for Cosmology and Particle Physics, Department of Physics, New York University, 4 Washington Pl, New York, NY 10003

² To whom correspondence should be addressed: morad.masjedi@physics.nyu.edu

³ Steward Observatory, 933 N Cherry Ave, Tucson, AZ 85721

⁴ Department of Astronomy, Case Western Reserve University, Cleveland, OH 44106

⁵ Max-Planck-Institut für Astronomie, Königstuhl 17, D-69117 Heidelberg, Germany

⁶ Department of Astronomy and Astrophysics, Pennsylvania State University, 525 Davey Laboratory, University Park, PA 16802

⁷ Theoretical Division, Los Alamos National Laboratory, Los Alamos, NM 87545

⁸ Apache Point Observatory, P.O. Box 59, Sunspot, NM 88349

Subject headings: cosmology: observations — galaxies: elliptical and lenticular, cD — galaxies: fundamental parameters — large-scale structure of universe — methods: statistical — surveys

1. INTRODUCTION

Galaxy clustering is a tool for the study of a diverse set of phenomena at different scales. On large scales (~ 100 Mpc) the density perturbations are small enough to be described in a linear framework, allowing analysis of cosmological models in detail and constraints on cosmological parameters (Tegmark et al. 2004a). In addition, recent studies have used extremely large-scale galaxy clustering to test fundamental cosmological hypotheses, such as homogeneity of the Universe (Hogg et al. 2005) and flatness of the universe (Eisenstein et al. 2005).

On intermediate scales (0.3 to 30 Mpc), galaxy clustering probes the relation of galaxies to dark matter through the biased clustering of dark matter halos. On these scales the two-point correlation function is found to be very close to a power law. Recent work has shown that the observed small deviations of the correlation function from a power-law on these scales can be interpreted in the framework of the Halo Occupation Distribution (HOD; Peacock & Smith 2000; Seljak 2000; Scoccimarro et al. 2001; Berlind & Weinberg 2002) as a natural transition between galaxy pairs within a single virialized halo and galaxy pairs in separate halos (e.g., Zehavi et al. 2004, 2005b).

On sufficiently small scales within a halo (< 1 Mpc), galaxy clustering will probe more than just the properties of the dark matter. On these scales one expects a variety of more complex processes to modify the galaxy clustering and thus presumably give rise to features in the correlation function $\xi(r)$. These processes include dynamical friction, tidal interactions, stellar feedback and other dissipative processes. These processes will force close galaxy pairs to merge over time-scales of order of the dynamical time ($\sim 10^8$ yr) (Toomre 1977; Larson & Tinsley 1978; van Dokkum 2005; Bell et al. 2005). Thus measurements of the correlation function $\xi(r)$ on small scales can be translated to a number density of near-future merger events. Some understanding of the merger process can be used to turn this density into a galaxy merger rate or at least a constraint thereon, providing an empirical measure of the importance of mergers as a fundamental mode of stellar mass addition to galaxies.

In addition, numerical simulations within the cold dark matter paradigm find that self-bound substructures within dark matter halos (subhalos) merge to form larger systems. It is

tempting to associate these subhalos with galaxies in groups and clusters (Klypin et al. 1999; Kravtsov & Klypin 1999; Colín et al. 1999; Moore et al. 1998b). Comparison between galaxy clustering and subhalo clustering on very small scales can lead to a better understanding of the connection between galaxies and dark matter subhalos (Kravtsov et al. 2004; Zentner et al. 2005).

There are no measurements of the real-space correlation function on scales smaller than 100 kpc. This is mainly due to the fact that on small angular separations the selection function of typical surveys becomes too complex and the pair counts are limited by shot noise. Gott & Turner (1979) and Maller et al. (2005) measured the angular correlation function for angular separations that, for the median redshift of their sample translates to $10 < r < 100$ kpc. They both find that the correlation function $\xi(r)$ power law extends down to these small scales. The drawback of these studies is that they measure only angular, not proper correlations, and they are difficult to interpret without precise knowledge of the radial selection function and density field.

The Sloan Digital Sky Survey (SDSS; York et al. 2000) has provided the largest spectroscopic sample ever of these massive galaxies; its special Luminous Red Galaxy (LRG) target selection Eisenstein et al. (2001) uses color to pre-select luminous early-type galaxies in a volume much larger than that of the SDSS Main sample. Because of their high luminosities, their association with massive halos, and their spectral uniformity, LRGs are extremely useful probes of large-scale structure. In addition, however, their morphological simplicity makes it straightforward to study their clustering at very small scales; Their lack of cold gas (and, indeed, the lack of equally bright blue galaxies) means that close passages and mergers do not trigger significant star formation, change the colors significantly, or change the morphology significantly, and therefore do not “remove” systems of interest at small scales from the parent sample. In this paper we capitalize on these properties of the LRGs—and the enormous volume of the SDSS LRG sample—to measure the clustering to extremely small scales (~ 10 kpc) and to constrain the LRG–LRG merger rate.

Throughout this paper all distances are comoving, calculated for a cosmological world model with $(\Omega_m, \Omega_\Lambda) = (0.3, 0.7)$ and Hubble constant parameterized by $H_0 \equiv 100 h \text{ km s}^{-1} \text{ Mpc}^{-1}$. At the mean redshift of the sample ($z \sim 0.3$), the fiber collision scale, 55 arcsec, corresponds to ~ 200 kpc and the SDSS median PSF width, 1.4 arcsec, translates to ~ 6 kpc.

2. DATA

The SDSS (Stoughton et al. 2002; Abazajian et al. 2003; Abazajian et al. 2004) is conducting an imaging survey of $\sim 10^4$ square degrees in 5 bandpasses: u , g , r , i , and z (Fukugita et al. 1996; Gunn et al. 1998, 2005). Photometric monitoring (Hogg et al. 2001), image processing (Lupton et al. 2001; Stoughton et al. 2002; Pier et al. 2003), and good photometric calibration (Smith et al. 2002; Ivezić et al. 2004) allow one to select galaxies (Strauss et al. 2002; Eisenstein et al. 2001), quasars (Richards et al. 2002), and stars for spectroscopic observations with the twin fiber-fed double-spectrographs.

Targets are assigned to spectroscopic fiber plug plates with a tiling algorithm that ensures nearly complete samples (Blanton et al. 2003a). The angular completeness is characterized carefully for each unique region of overlapping spectroscopic plates (“sector”) on the sky. An operational constraint of SDSS spectrographs is that the physical size of the fiber coupling forces the angular separation of the targets to be larger than 55 arcsec. This “fiber collision” constraint is partly reduced by having roughly one third of the sky covered by overlapping plates, but it still results in $\sim 7\%$ of targeted galaxies not having measured redshifts.

We focus here on the Luminous Red Galaxy spectroscopic sample (Eisenstein et al. 2001). This sample is constructed from color-magnitude cuts in g , r , and i to select galaxies that are likely to be luminous early-type galaxies at redshifts between 0.15 and 0.5. The selection is highly efficient and the redshift success rate is excellent. The sample is constructed to be close to volume-limited up to $z = 0.36$, with a dropoff in density toward $z = 0.5$.

This study uses a sample drawn from NYU LSS `sample14` (Blanton et al. 2005) and covers 3,836 square degrees containing 55,000 LRGs between redshift of 0.16 and 0.47. The subsample of LRGs used in this paper has luminosity and redshift ranges of $-23.2 < M_g < -21.2$ and $0.16 < z < 0.36$, respectively. The absolute magnitudes include Galactic extinction corrections (Schlegel et al. 1998), k -corrections and passive evolution corrections to redshift $z = 0.3$. This subsample, which is chosen to maximize our use of the volume-limited portion of the LRG spectroscopic sample, is identical to the first subsample (29298 galaxies) used in Zehavi et al. (2005a), with the difference that in this paper we limit ourself only to the North Galactic Cap (24520 galaxies). This is due to the slight difference in some aspects of tiling and photometric calibrations between the North and South Galactic Cap areas. The details of the radial and angular selection functions are described elsewhere (Zehavi et al. 2005a).

We create large catalogs of randomly distributed points based on these angular and radial models. These catalogs match the redshift distribution of the LRGs and are isotropic

within the survey region. These catalogs allow us to check the survey completeness of any given volume and provide a homogeneous baseline (e.g., expected numbers) for the tests that follow.

3. METHOD & RESULTS

3.1. Projected Correlation Function

To calculate the real-space correlation function on intermediate scales, one estimates the correlation function on a two-dimensional grid of pair separations parallel (π) and perpendicular (r_p) to the line of sight, termed $\xi(r_p, \pi)$. This can be turned into projected correlation function

$$w_p(r_p) = 2 \int_0^{\pi_{max}} d\pi \xi(r_p, \pi). \quad (1)$$

in which π_{max} is set to a value sufficiently large to include most correlated pairs and give stable results (i.e., independent of the choice of π_{max} within the error-bars). Using this method, Zehavi et al. (2005a) calculate $w_p(r_p)$ for the LRG sample in the range $0.3 \text{ Mpc} \lesssim r_p \lesssim 30 \text{ Mpc}$. The lower limit in the Zehavi et al. (2005a) analysis was set to eliminate the incompleteness effects that are introduced by the 55 arcsec fiber collision radius.

We overcome the fiber collision problem by cross correlating the spectroscopic sample with the full sample of LRG targets in the SDSS imaging, whether or not they have observed redshifts. To do this we use the Zehavi et al. (2005a) subsample of LRGs (as explained above) as our spectroscopic sample, and *all* LRG targets as our imaging sample. For each LRG from the spectroscopic sample, we treat the nearby imaging LRGs (whether they have spectrum or not) as if they are at the same redshift as the spectroscopically observed LRG. This allows us to calculate a g -band absolute magnitude (M_g) for them in the same manner as the LRGs with spectra and choose the ones that make it inside the sample limits (e.g., $-23.2 < M_g < -21.2$). This turns our cross-correlation into an auto-correlation. In addition, assuming the LRG redshift we can bin the pairs according to their comoving projected separation.

We statistically remove the interlopers, i.e., galaxies not at the same redshift but treated as such by the algorithm, by making random spectroscopic samples with the same redshift distribution as LRG spectroscopic sample and cross-correlating this sample with the imaging LRG sample. We subtract the scaled random interlopers from our data-data correlation.

This method makes use of the fact that essentially all the support for the projected

correlation function w_p integral (1) arises from line-of-sight separations π that are much smaller than the distance to the given galaxy. The downside to this method is the loss of signal-to-noise due to interlopers, which becomes irrelevant at small-scales, where the correlation function becomes much larger than unity.

Using this method we calculate $w_p(r_p)$; schematically:

$$n w_p(r_p) = \frac{D_s D_i}{D_s R_i} - \frac{R_s D_i}{R_s R_i} \quad , \quad (2)$$

where n is the average comoving density of the spectroscopic LRG sample used here, D_s and D_i are the spectroscopic and imaging data samples, and R_s and R_i are the random spectroscopic and random imaging samples. In detail, the factors are:

$$D_s D_i = \frac{\sum_{j \in D_s D_i \text{ pairs}} p_j}{\sum_{j \in D_s} p_j} \quad , \quad (3)$$

where p_j is the weight given to each spectroscopic LRG to account for the fiber collisions. We calculate this weight by running a friends-of-friends grouping algorithm with a 55 arcsec linking length provided within `sample14` package. Within each “collision group” made by the friends-of-friends we find the number of objects that with spectroscopic redshifts and divide by the total number. The inverse of this ratio is the weighting p_j assigned to each spectroscopic LRG. This procedure emulates the SDSS tiling algorithm (Blanton et al. 2003a).

$$D_s R_i = \frac{\sum_{j \in D_s R_i \text{ pairs}} p_j}{\sum_{j \in D_s} p_j \left(\frac{d\Omega}{dA} \right)_j \frac{dN}{d\Omega}} \quad , \quad (4)$$

where $\left(\frac{d\Omega}{dA} \right)_j$ is the inverse square of the comoving distance to spectroscopic galaxy j and $\frac{dN}{d\Omega}$ is the number density of the random imaging catalog per solid angle. The average of multiplication of these two terms gives the average number of random imaging objects per unit comoving area around each spectroscopic galaxy.

$$R_s D_i = \frac{\sum_{j \in R_s D_i \text{ pairs}} f_j}{\sum_{j \in R_s} f_j} \quad , \quad (5)$$

where f_j is the weight given to spectroscopic galaxy j which accounts for the incompleteness of the spectroscopic survey in that region of the sky *not* due to fiber collision but due to all the other selection effects in survey. The `sample14` package provides the angular geometry of the spectroscopic survey expressed in terms of spherical polygons. The geometry is complicated: the spectroscopic plates are circular and overlap, while the imaging is in long strips on the sky, and there are some overlap regions of certain plates that may not have been yet observed. The resulting spherical polygons track all these effects and characterize the geometry in terms of “sectors”, each being a unique region of overlapping spectroscopic plates. In each sector, we count the number of possible targets (LRG, MAIN, and quasar), excluding those missed because of fiber collisions, and the number of these whose redshifts were determined. We weight the random spectroscopic LRGs by the inverse of the ratio of these numbers (f_j). In truth, the priority of all targets are not equal, such that LRGs will always lose to quasar candidates, but the LRG priority is equal to the dominant MAIN targets. Only about 12% of the fibers are assigned to quasars, hence quasar LRG collisions are rare and this priority bias could be ignored.

$$R_s R_i = \frac{\sum_{j \in R_s R_i \text{ pairs}} f_i}{\sum_{j \in R_s} f_j \left(\frac{d\Omega}{dA} \right)_j \frac{dN}{d\Omega}} \quad , \quad (6)$$

is similar to equation 4 but for the random Spectroscopic and random imaging pairs.

Figure 1 shows the projected correlation function measured in this manner (data in Table 1). The error-bars are estimated using jackknife resampling covariance matrix with 50 subsamples. These results agree well with Zehavi et al. (2005a) on their overlap range (0.3 to $8 h^{-1}$ Mpc) and on smaller scales (0.01 to $0.3 h^{-1}$ Mpc) is very close to an extension of the best-fit power-law from Zehavi et al. (2005a).

3.2. Test on Mock LRG Catalogs

To test our method, we use an N-body simulation of a Λ CDM cosmological model, with $\Omega_m = 0.3$, $\Omega_\Lambda = 0.7$, $\Omega_b = 0.04$, $h \equiv H_0 / (100 \text{ km s}^{-1} \text{ Mpc}^{-1}) = 0.7$, $n_s = 1.0$, and $\sigma_8 = 0.9$. This model is in good agreement with a wide variety of cosmological observations (see, e.g., Spergel et al. 2003; Tegmark et al. 2004b; Abazajian et al. 2005). Initial conditions were set up using the transfer function calculated for this cosmological model by CMBFAST (Seljak & Zaldarriaga 1996). The simulation was run at Los Alamos National Laboratory (LANL) using the Hashed-Oct-Tree (HOT) code (Warren & Salmon 1991); the simulation followed the

evolution of 1024^3 dark matter particles, each of mass $3.51 \times 10^{10} h^{-1} M_{\odot}$, in a comoving box of size $768 h^{-1} \text{Mpc}$. The gravitational force softening is $\epsilon_{\text{grav}} = 12 h^{-1} \text{Kpc}$ (Plummer equivalent). We identify halos in the dark matter particle distributions using a friends-of-friends algorithm with a linking length equal to 0.2 times the mean inter-particle separation. We populate these halos with galaxies using a simple model for the Halo Occupation Distribution (HOD). Every halo with a mass M greater than a minimum mass M_{min} is assigned a central galaxy that is placed at the halo center of mass and is given the mean halo velocity. A number of satellite galaxies is then drawn from a Poisson distribution with mean $((M - M_{\text{min}})/M_1)^{\alpha}$, for $M \geq M_{\text{min}}$. These satellite galaxies are assigned the positions and velocities of randomly selected dark matter particles within the halo. We select the parameter values $M_{\text{min}} = 4.5 \times 10^{13} h^{-1} M_{\odot}$, $M_1 = 3.5 \times 10^{15} h^{-1} M_{\odot}$, and $\alpha = 1$ that yield a mock galaxy population with the observed space density of LRGs and approximately the correct galaxy-galaxy correlation function.

In order to carve the SDSS LRG sample geometry out of our mock cube, we create a new cube with 27 times larger volume by tiling the mock cube $3 \times 3 \times 3$. Since the N-body simulation used to construct the mock was run with periodic boundary conditions, we can tile the cube without having density discontinuities at the boundaries. We set the center of this tiled cube to be the origin and put galaxies into redshift space using the line-of-sight component of their peculiar velocities. We then compute RA, Dec, and redshift coordinates for every mock galaxy in the tiled cube. Finally, we only keep galaxies whose coordinates would place them within the LRG sample geometry. The final step in creating a mock LRG catalog is to incorporate the fiber collision constraint. In the SDSS, LRG fibers collide both with each other, and with other galaxies that are mostly uncorrelated foreground galaxies. We create a foreground screen of mock galaxies on the sky by populating the same N-body simulation with a different HOD that yields an angular correlation function equal to the mean for all SDSS galaxies. We then allow all galaxies to collide with each other and keep track of collided mock LRG galaxies. This approach produces results that are very close to the SDSS tiling algorithm (Blanton et al. 2003a).

We use this mock to test two different aspect of our correlation estimator: the cross-correlation method and the fiber collision weighting scheme. First we use all the mock galaxies as both our spectroscopic and imaging samples (no galaxies eliminated by fiber collisions). Next we drop the galaxies that would not get a redshift in SDSS due to fiber collision from our spectroscopic sample and repeat the test. Figure 2 shows the measured projected correlation function for both cases in comparison to the real projected correlation function for the full cube of the mock. It is worth noting that on very small scales the shot noise dominates the galaxy pair counts and limits the comparison.

3.3. Photometry Test

One important issue with all clustering measurements on small scales is possible photometric biases when measuring close pairs. This may emerge when the outskirts of a pair of galaxies overlap on these scales. This can lead to biased flux measurements for galaxies which will affect the completeness of the samples. To estimate the magnitude of this effect for SDSS, we ran a simulation in which we create fake images of pairs of galaxies with separations ranging from 2 to 35 arcsec. We studied two different cases, one for galaxy pairs consisting of two identical galaxies and another with galaxies of different luminosities. The basic information regarding these galaxies is summarized in Table 2. These galaxies represent passively evolving LRG galaxies observed at a redshift of $z = 0.3$ with de Vaucouleurs profiles ($n = 4$ Sérsic profiles).

We place one such galaxy pair onto RUN 2662 of SDSS imaging. This RUN has a typical SDSS seeing of about 1 arcsec. Each galaxy image is convolved with the local seeing of the field. The flat fielding vectors and gain corrections applied to the SDSS imaging in reverse to each constructed image. After inserting known bad pixels into the mock galaxy images; these images are added to raw SDSS images. These new images are then processed using the standard SDSS pipeline, PHOTO, to determine the effect of proximity of galaxies on their measured properties.

We found that for the case of two identical galaxies, for separations below 3 arcsec, the two galaxies are not well deblended, leading to the detection of a single galaxy with combined flux of the individual galaxies. At separations larger than 20 arcsec, the Petrosian flux measures 79.5 percent of the input Sérsic flux (as expected) and the ratio of the recovered to input flux is independent of the separation. In other words, in the absence of a close neighbor for a $n = 4$ Sérsic galaxy, the Petrosian flux only measures about 80 percent of a galaxy’s light. For intermediate separations, ($5 < s < 20$ arcsec), the fraction of the recovered flux to input flux increases to 83 percent. This increase is likely due to a double counting of the low level diffuse emission from the two galaxies which is being poorly deblended between the two objects. Figure 3 shows this result.

Using this result we correct for the completeness of our sample on small scales. We convert angular separation to projected separation using the median redshift of the sample $z = 0.3$ (the same redshift is used for the test). In addition we know from Eisenstein et al. (2001) that for each 0.1 magnitude change of the faint limit of our sample the number of galaxies in the samples is increased by roughly 30 percent. For each projected distance separation r_p bin in the projected correlation function $w_p(r_p)$ we convert the excess flux count for that separation to an excess of galaxy counts in the sample. The square of this quantity will be the excess in galaxy pairs allocated to that separation bin. we then correct

our projected correlation function by this factor for each given separation (Figure 1, Table 1). The result for the second case with galaxies of different magnitudes is close enough to the first case that we use only the first case to correct our sample.

3.4. Real-Space Correlation Function

The projected correlation function $w_p(r_p)$ can be “deprojected” to get $\xi(r)$ by

$$\xi(r) = -\frac{1}{\pi} \int_r^\infty dr_p \frac{dw_p(r_p)}{dr_p} (r_p^2 - r^2)^{-1/2} \quad (7)$$

(e.g., Davis & Peebles 1983). We calculate this integral analytically by linear interpolation between the binned $w_p(r_p)$ values, following Saunders et al. (1992). This estimate is only accurate to a few percent, due to limitations of the interpolation.

Figure 4 shows the real-space correlation function, obtained in this fashion, combined with the real-space correlation function $\xi(r)$ on intermediate-scales from Zehavi et al. (2005a) and redshift-space correlation function $\xi(s)$ on large-scales from Eisenstein et al. (2005) for the LRG sample. Also shown are the power-law $\xi(r) = [r/(10 h^{-1} Mpc)]^{-2.0}$ and the “1-halo term” of the correlation function (which only counts pairs of galaxies within the same dark matter halo) calculated for the HOD parameters given by Zehavi et al. (2005b) for the $M_r < -22$ SDSS MAIN sample which is close to the LRG sample.

Figure 5 shows the real space correlation function divided by a r^{-2} power-law to accentuate the deviations from a power-law. The dip at 1 Mpc is described and quantified by the halo model as the transition from 2-halo to 1-halo term (Zehavi et al. 2004). The upturn at 0.03 Mpc could be real but is not highly significant. Finally the drop of the innermost point at 0.01 Mpc is most probably due to deblending issues.

3.5. Merger Rate

If we interpret the LRG correlation function $\xi(r)$, measured at small scales as a quasi-steady-state inflow leading to the mergers of pairs of LRGs, we can straightforwardly turn the measured $\xi(r)$ into a merger rate.

We assume that there is a length scale r_f inside of which dynamical friction is so effective

that pairs at this separation merge in a dynamical time t_{dyn} , where the dynamical time is

$$t_{\text{dyn}} \approx \frac{2\pi r_f}{v_{\text{circ}}} \quad , \quad (8)$$

and v_{circ} is the circular velocity of the orbit, which is roughly 1.5 times the velocity dispersion σ_v ; the exact value of the numerical factor depends on the velocity ellipsoid. For typical velocity dispersions, $\sigma_v \sim 200 \text{ km s}^{-1}$, and merger length scales, $r_f \sim 10 \text{ kpc}$, we find a dynamical time $t_{\text{dyn}} \sim 200 \text{ Myr}$, which is in agreement with time-scales derived by Bell et al. (2005) from merger simulations.

If the number density of LRGs is n_{LRG} , the average number N_f within distance r_f of any “target” LRG is

$$N_f \approx 4\pi n_{\text{LRG}} \int_0^{r_f} r^2 \xi(r) dr \quad . \quad (9)$$

and the LRG merger rate Γ_{LRG} is, by assumption

$$\Gamma_{\text{LRG}} = \frac{N_f}{t_{\text{dyn}}} \approx 3 r_f^2 \xi(r_f) n_{\text{LRG}} \sigma_v \quad . \quad (10)$$

In this derivation we have used the fact that the $\xi(r) \sim r^{-2}$ (Figure 5). This merger rate can be written as

$$\Gamma_{\text{LRG}} \approx \frac{1}{160 \text{ Gyr}} \left[\frac{r_f^2 \xi(r_f)}{100 \text{ Mpc}^2} \right] \left[\frac{\sigma_v}{200 \text{ km s}^{-1}} \right] \left[\frac{n_{\text{LRG}}}{10^{-4} \text{ Mpc}^{-3}} \right] \quad , \quad (11)$$

which is equivalent to a comoving volume merger rate of:

$$\dot{\phi}_M \equiv \frac{\Gamma_{\text{LRG}}}{n_{\text{LRG}}} \sim 0.6 \times 10^4 \text{ Gyr}^{-1} \text{ Gpc}^{-3} \quad . \quad (12)$$

This merger rate does not depend on the choice of r_f which is indeed poorly known. It is worth noting that this merger rate is a strict upper limit. First, we assume that all close pairs will merge, but in principle galaxies in high density clusters could pass by each other without merging. Secondly, we are assuming that all galaxies will merge in a dynamical time, which is the minimum possible time for a merger to occur.

4. DISCUSSION

We have combined the data for 24520 luminous red galaxies from the SDSS spectroscopic sample with LRG targets in the SDSS imaging sample to measure the strength of clustering

for LRGs on small scales (0.01 to $8 h^{-1}$ Mpc). We deal with the fiber collision incompleteness of the SDSS spectroscopic sample on scales smaller than 55 arcsec by cross-correlating the spectroscopic and imaging samples and statistically removing the interloping galaxies. This method is extremely powerful on small scales at which the correlation function becomes much larger than unity.

We find that the correlation function on these scales is very close to an extrapolation of the correlation function power-law found on larger scales $\xi(r) \propto r^{-2}$ (Zehavi et al. 2005a). This is surprising, as one might expect the direct interactions between galaxies (e.g., dynamical friction, galaxy merger, tidal impulses, etc.) to create features in the correlation function.

This result cannot be simply explained with the current best-fit of the of Halo Occupation Distribution (HOD) models for galaxy clustering (e.g., Zehavi et al. 2005a; Tinker et al. 2005a). This inconsistency arises from the fact that in current HOD models the galaxy-galaxy correlation function on small scales simply follows the convolution of the dark matter halo profile with itself (1-halo term). For an NFW profile (Navarro et al. 1997) this relation is proportional to r^{-1} toward the core of the halo and similarly for the Moore profile (Moore et al. 1998a) produces a $r^{-1.5}$ relation; neither is sufficiently steep to fit the results of this paper. Figure 4 shows the 1-halo term of the correlation function calculated for the HOD parameters given in Zehavi et al. (2005b). If HOD models are modified to have a galaxy distribution much more concentrated than the dark matter or to have dark matter halos with density profiles much steeper than NFW toward the core of the halo, this result could in principle be accommodated within HOD models.

We convert the correlation function on these scales to statistics of galaxies in close dynamical pairs, and we infer an LRG-LRG merger rate of $\lesssim 1/160 \text{ Gyr}^{-1}$ or a comoving volume merger rate, $\dot{\phi}_M \sim 0.6 \times 10^4 \text{ Gyr}^{-1} \text{ Gpc}^{-3}$. The fact that in large clusters, galaxies can closely pass each other without merging, turns any merger rate inferred from close dynamical pair statistics into an strict upper limit. This upper limit on the LRG merger rate could in principle be violated if the merger process triggers such strong star-formation activities in these galaxies that they become too blue to make it to the LRG sample selection cuts. However, this proposal is not tenable, as LRGs contain little apparent gas or dust and essentially there are no blue galaxies with luminosities comparable to the LRGs (Blanton et al. 2003b; Eisenstein et al. 2001). Therefore the LRG merger rate is in fact very close to merger rate for all galaxies with LRG luminosities regardless of their color.

In previous work, there are two main methods for measuring merger rates, the most popular one is to convert the close pair statistics to a merger rate (e.g., Zepf & Koo 1989; Burkey et al. 1994; Patton et al. 1997, 2000; Carlberg et al. 2000; Bell et al. 2005). The other

method uses the asymmetry parameter (A) to determine the fraction of galaxies undergoing mergers (Conselice et al. 2003a,b; van Dokkum 2005). It is difficult to compare these previous studies of the merger rate with that found here because our LRG sample is more luminous and has a significantly smaller number density than the samples used in those studies. The merger rate has been found to be higher for higher redshifts and higher for fainter samples (Conselice et al. 2003a). For this reason, an SDSS-size sample was required to measure the merger rate for LRG type galaxies at low redshifts. Nevertheless our result is, in principal, consistent with the extrapolation of the best fits to samples at higher redshifts or fainter samples (Conselice 2005).

One question to address by merger-rate measurements is the importance of major mergers in the mass build-up of massive galaxies. This could be answered by measuring the cross-correlation of galaxies of different mass with LRGs on small scales to obtain a mass spectrum for objects merging into LRGs. Murali et al. (2002) created a simulation for L^* galaxies to answer this question. They find that smooth accretion plays the dominant role in mass build-up. Unfortunately the resolution of the simulation ($L \sim L^*/4$) was too close to the galaxies in question to be able to distinguish true smooth accretion from mergers with objects below the mass resolution. LRGs are massive enough that the merger of objects far below their mass could be studied in hydro-dynamical simulations to give a detailed mass spectrum for merger events.

It is a pleasure to thank Jim Peebles, Sebastian Pueblas, David Schlegel, and Roman Scoccimarro for valuable discussions and software. MM, DWH, MRB, and AB are partially supported by NASA (NAG5-11669) and NSF (AST-0428465). This research made use of the NASA Astrophysics Data System.

Funding for the creation and distribution of the SDSS Archive has been provided by the Alfred P. Sloan Foundation, the Participating Institutions, the National Aeronautics and Space Administration, the National Science Foundation, the U.S. Department of Energy, the Japanese Monbukagakusho, and the Max Planck Society. The SDSS Web site is “<http://www.sdss.org/>”.

The SDSS is managed by the Astrophysical Research Consortium for the Participating Institutions. The Participating Institutions are The University of Chicago, Fermilab, the Institute for Advanced Study, the Japan Participation Group, The Johns Hopkins University, the Korean Scientist Group, Los Alamos National Laboratory, the Max-Planck-Institute for Astronomy, the Max-Planck-Institute for Astrophysics, New Mexico State University, University of Pittsburgh, University of Portsmouth, Princeton University, the United States Naval Observatory, and the University of Washington.

REFERENCES

- Abazajian, K. et al. 2003, *AJ*, 126, 2081
- Abazajian, K. et al. 2004, *AJ*, 128, 502
- Abazajian, K. et al. 2005, *AJ*, 129, 1755
- Bell, E. F. et al. 2005, *ArXiv Astrophysics e-prints*
- Berlind, A. A. & Weinberg, D. H. 2002, *ApJ*, 575, 587
- Blanton, M. R., Lin, H., Lupton, R. H., Maley, F. M., Young, N., Zehavi, I., & Loveday, J. 2003a, *AJ*, 125, 2276
- Blanton, M. R., Schlegel, D. J., Strauss, M. A., Brinkmann, J., Finkbeiner, D., Fukugita, M., Gunn, J. E., Hogg, D. W., Ivezić, Ž., Knapp, G. R., Lupton, R. H., Munn, J. A., Schneider, D. P., Tegmark, M., & Zehavi, I. 2005, *AJ*, 129, 2562
- Blanton, M. R. et al. 2003b, *ApJ*, 594, 186
- Burkey, J. M., Keel, W. C., Windhorst, R. A., & Franklin, B. E. 1994, *ApJ*, 429, L13
- Carlberg, R. G., Yee, H. K. C., Morris, S. L., Lin, H., Hall, P. B., Patton, D., Sawicki, M., & Shepherd, C. W. 2000, *ApJ*, 542, 57
- Colín, P., Klypin, A. A., Kravtsov, A. V., & Khokhlov, A. M. 1999, *ApJ*, 523, 32
- Conselice, C. J. 2005, *ArXiv Astrophysics e-prints*
- Conselice, C. J., Bershady, M. A., Dickinson, M., & Papovich, C. 2003a, *AJ*, 126, 1183
- Conselice, C. J., Chapman, S. C., & Windhorst, R. A. 2003b, *ApJ*, 596, L5
- Davis, M. & Peebles, P. J. E. 1983, *ApJ*, 267, 465
- Eisenstein, D. J. et al. 2001, *AJ*, 122, 2267
- Eisenstein, D. J. et al. 2005, *ApJ*, submitted (astro-ph/0501171)
- Fukugita, M., Ichikawa, T., Gunn, J. E., Doi, M., Shimasaku, K., & Schneider, D. P. 1996, *AJ*, 111, 1748
- Gott, J. R. & Turner, E. L. 1979, *ApJ*, 232, L79
- Gunn, J. E., Carr, M. A., Rockosi, C. M., Sekiguchi, M., et al. 1998, *AJ*, 116, 3040

- Gunn, J. E. et al. 2005, AJ, submitted
- Hoessel, J. G., Gunn, J. E., & Thuan, T. X. 1980, ApJ, 241, 486
- Hogg, D. W., Eisenstein, D. J., Blanton, M. R., Bahcall, N. A., Brinkmann, J., Gunn, J. E., & Schneider, D. P. 2005, ApJ, 624, 54
- Hogg, D. W., Finkbeiner, D. P., Schlegel, D. J., & Gunn, J. E. 2001, AJ, 122, 2129
- Ivezić, Ž. et al. 2004, Astronomische Nachrichten, 325, 583
- Klypin, A., Gottlöber, S., Kravtsov, A. V., & Khokhlov, A. M. 1999, ApJ, 516, 530
- Kravtsov, A. V., Berlind, A. A., Wechsler, R. H., Klypin, A. A., Gottlöber, S., Allgood, B., & Primack, J. R. 2004, ApJ, 609, 35
- Kravtsov, A. V. & Klypin, A. A. 1999, ApJ, 520, 437
- Larson, R. B. & Tinsley, B. M. 1978, ApJ, 219, 46
- Lupton, R. H., Gunn, J. E., Ivezić, Z., Knapp, G. R., Kent, S., & Yasuda, N. 2001, in ASP Conf. Ser. 238: Astronomical Data Analysis Software and Systems X, Vol. 10, 269
- Maller, A. H., McIntosh, D. H., Katz, N., & Weinberg, M. D. 2005, ApJ, 619, 147
- Moore, B., Governato, F., Quinn, T., Stadel, J., & Lake, G. 1998a, ApJ, 499
- Moore, B., Lake, G., & Katz, N. 1998b, ApJ, 495, 139
- Murali, C., Katz, N., Hernquist, L., Weinberg, D. H., & Davé, R. 2002, ApJ, 571, 1
- Navarro, J. F., Frenk, C. S., & White, S. D. M. 1997, ApJ, 490, 493
- Patton, D. R., Carlberg, R. G., Marzke, R. O., Pritchett, C. J., da Costa, L. N., & Pellegrini, P. S. 2000, ApJ, 536, 153
- Patton, D. R., Pritchett, C. J., Yee, H. K. C., Ellingson, E., & Carlberg, R. G. 1997, ApJ, 475, 29
- Peacock, J. A. & Smith, R. E. 2000, MNRAS, 318, 1144
- Pier, J. R., Munn, J. A., Hindsley, R. B., Hennessy, G. S., Kent, S. M., Lupton, R. H., & Ivezić, Ž. 2003, AJ, 125, 1559
- Postman, M. & Lauer, T. R. 1995, ApJ, 440, 28

- Richards, G. et al. 2002, *AJ*, 123, 2945
- Sandage, A. 1972, *ApJ*, 178, 1
- Saunders, W., Rowan-Robinson, M., & Lawrence, A. 1992, *MNRAS*, 258, 134
- Schlegel, D. J., Finkbeiner, D. P., & Davis, M. 1998, *ApJ*, 500, 525
- Schneider, D. P., Gunn, J. E., & Hoessel, J. G. 1983, *ApJ*, 264, 337
- Scoccamarro, R., Sheth, R. K., Hui, L., & Jain, B. 2001, *ApJ*, 546, 20
- Seljak, U. 2000, *MNRAS*, 318, 203
- Seljak, U. & Zaldarriaga, M. 1996, *ApJ*, 469, 437
- Smith, J. A., Tucker, D. L., et al. 2002, *AJ*, 123, 2121
- Spergel, D. N. et al. 2003, *ApJS*, 148, 175
- Stoughton, C. et al. 2002, *AJ*, 123, 485
- Strauss, M. A. et al. 2002, *AJ*, 124, 1810
- Tegmark, M. et al. 2004a, *Phys. Rev. D*, 69, 103501
- Tegmark, M. et al. 2004b, *ApJ*, 606, 702
- Tinker, J. L. et al. 2005a, *ApJ*, 631, 41
- Toomre, A. 1977, in *Evolution of Galaxies and Stellar Populations*, 401–+
- van Dokkum, P. G. 2005, *ArXiv Astrophysics e-prints*
- Warren, M. S. & Salmon, J. K. 1991, *BAAS*, 23, 1345
- York, D. et al. 2000, *AJ*, 120, 1579
- Zehavi, I., Eisenstein, D. J., Nichol, R. C., Blanton, M. R., Hogg, D. W., Brinkmann, J., Loveday, J., Meiksin, A., Schneider, D. P., & Tegmark, M. 2005a, *ApJ*, 621, 22
- Zehavi, I. et al. 2004, *ApJ*, 608, 16
- Zehavi, I. et al. 2005b, *ApJ*, 630, 1
- Zentner, A. R., Berlind, A. A., Bullock, J. S., Kravtsov, A. V., & Wechsler, R. H. 2005, *ApJ*, 624, 505

Zepf, S. E. & Koo, D. C. 1989, ApJ, 337, 34

Correlation Function Measurements			
separation (h^{-1} Mpc)	$w_p(r_p)$ (h^{-1} Mpc)	$\xi(r)$	Photometric Correction
0.010	7060(2300)	−63040(130000)	3.177
0.017	20570(3500)	471600(120000)	1.685
0.026	10950(2200)	146300(49000)	1.331
0.042	5387(850)	35400(12000)	1.258
0.066	3950(600)	17100(4900)	1.096
0.105	2631(310)	6865(1800)	0.997
0.166	1637(180)	2366(590)	1.000
0.263	1161(78)	1152(190)	1.000
0.417	795.7(48)	627.1(66)	1.000
0.660	412.8(27)	180.4(17)	1.000
1.047	246.4(19)	61.14(7.5)	1.000
1.659	162.6(12)	24.19(2.7)	1.000
2.629	115.3(11)	12.23(1.2)	1.000
4.167	77.15(9.7)	5.677(0.52)	1.000
6.604	52.31(8.2)	2.320(.19)	1.000

Table 1: Measurements of the projected correlation function, $w_p(r_p)$, and real-space correlation function, $\xi(r)$ for the LRG sample. The diagonal terms of the measurements error covariance matrices are given in parentheses.

Properties of the Simulated Galaxies						
M_r	Half-Light Radius	m_r	$u - r$	$g - r$	$r - i$	$i - z$
−22.5	(10, 3.2)	17.867	3.831	1.722	0.581	0.955
−22.0	(7, 2.24)	18.367	3.831	1.722	0.581	0.955

Table 2: Properties of the fake galaxies made for the photometry test. The half-light radius is given in comoving kpcs and arcseconds.

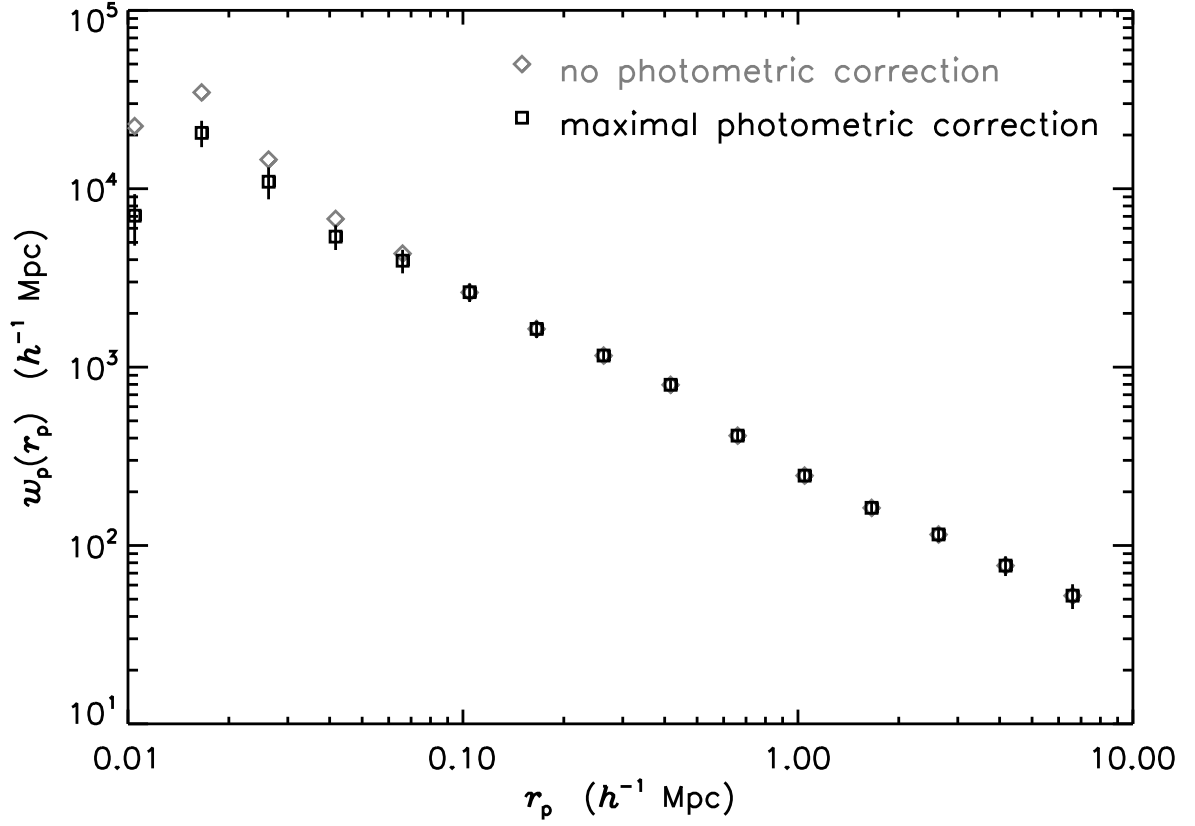


Fig. 1.— Projected correlation function $w_p(r_p)$ for the LRG sample ($-23.2 < M_g < -21.2$ and $0.16 < z < 0.36$) calculated as described in the text. The gray diamonds show the measured projected correlation function before correction for the photometric bias in the close galaxy pairs. The error-bars are from the jackknife error covariance matrix.

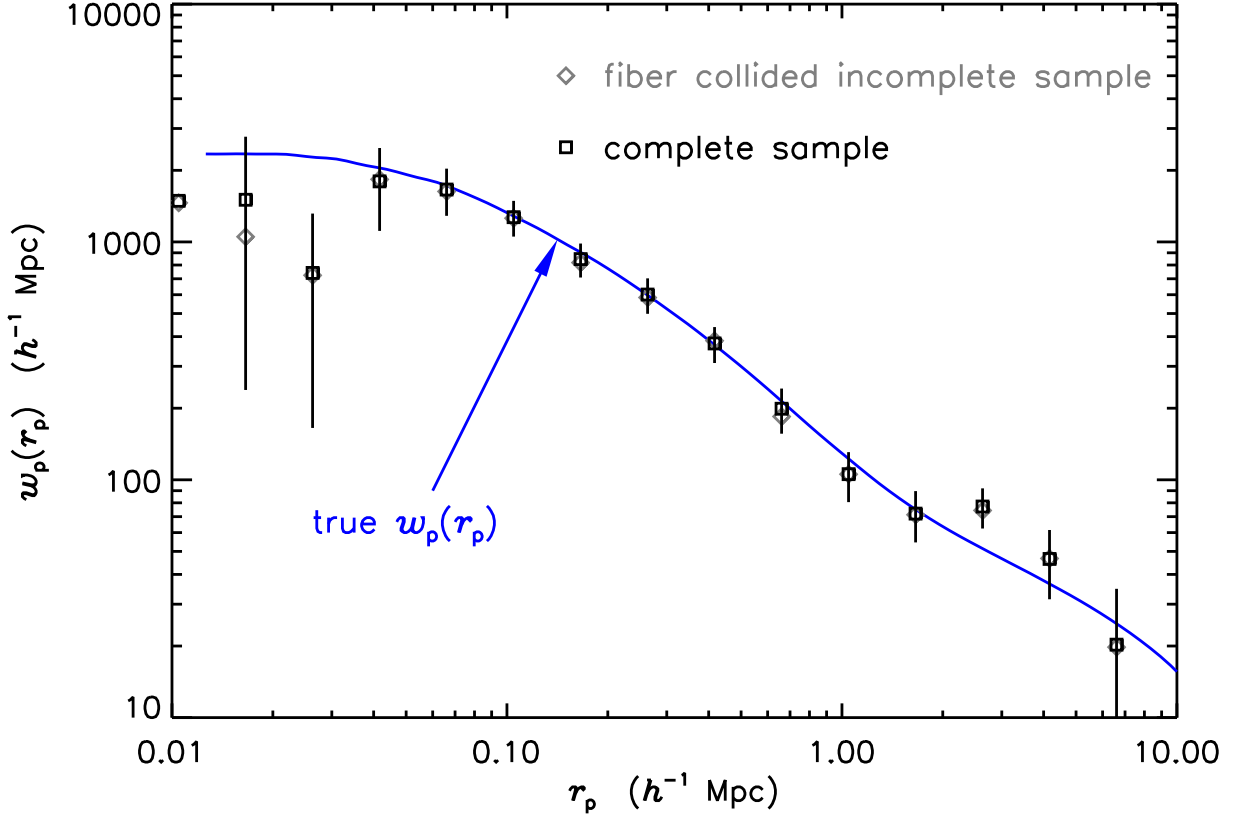


Fig. 2.— Projected correlation function $w_p(r_p)$ measured for the mock cube measured directly in the simulation (solid line), and by the method described in the text after applying SDSS geometry cuts (black squares). The gray diamonds show the measured $w_p(r_p)$ for the mock after applying the SDSS geometry cuts and the fiber collision incompleteness. It is worth noting that the geometry cuts select about a third of all galaxies in the cube therefore on very small scales the data points are dominated by the shot noise.

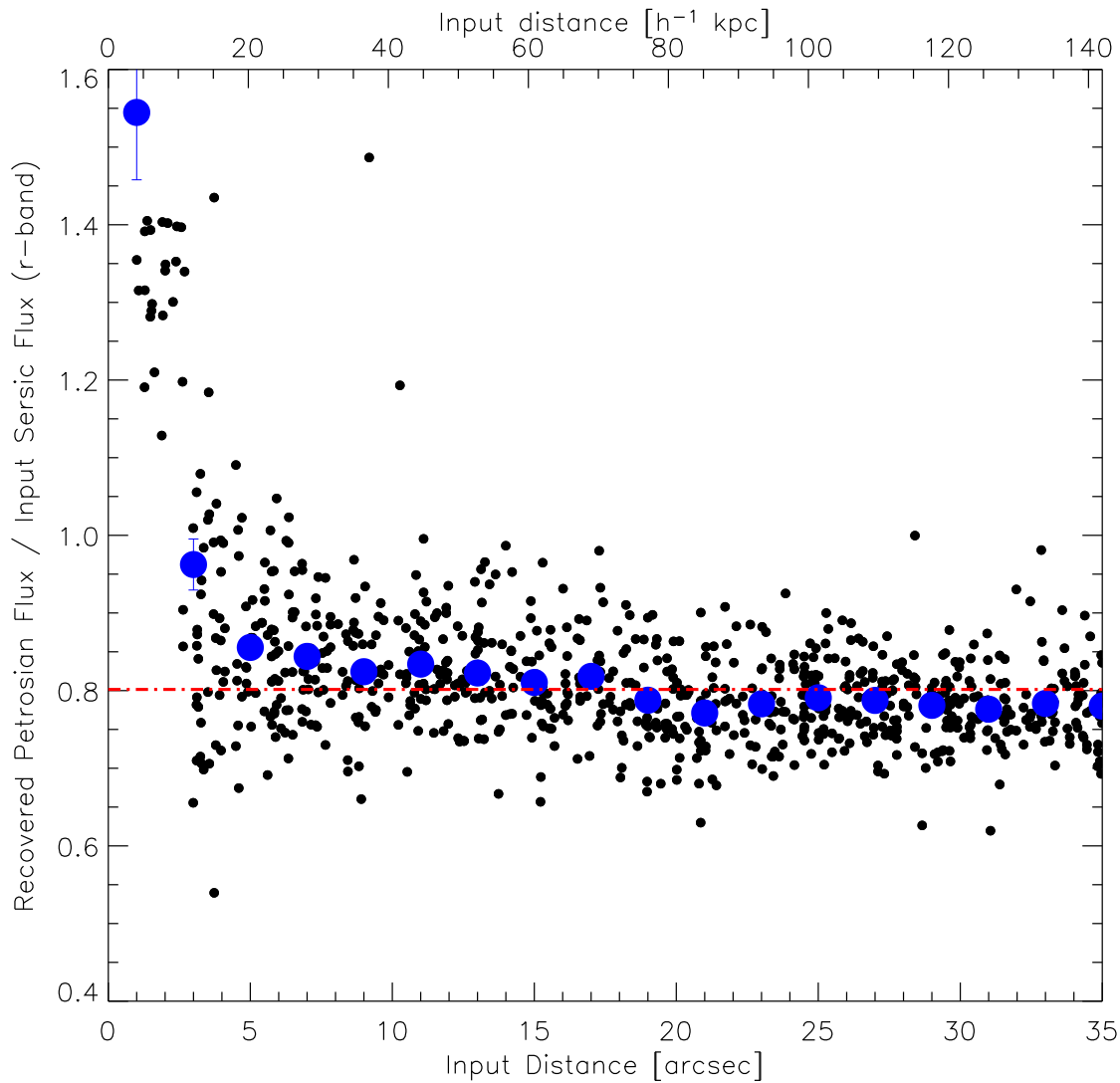


Fig. 3.— Recovered Petrosian flux to input Sérsic flux as a function of the separation of the two galaxies in the pair, the blue dots show the three sigma out-layer rejected average of the recovered flux for different separations. It can be seen that the pipeline completely fails for galaxies closer than 3 arcsec and on average there is an excess in the recovered flux of galaxies separated by less than 20 arcsec.

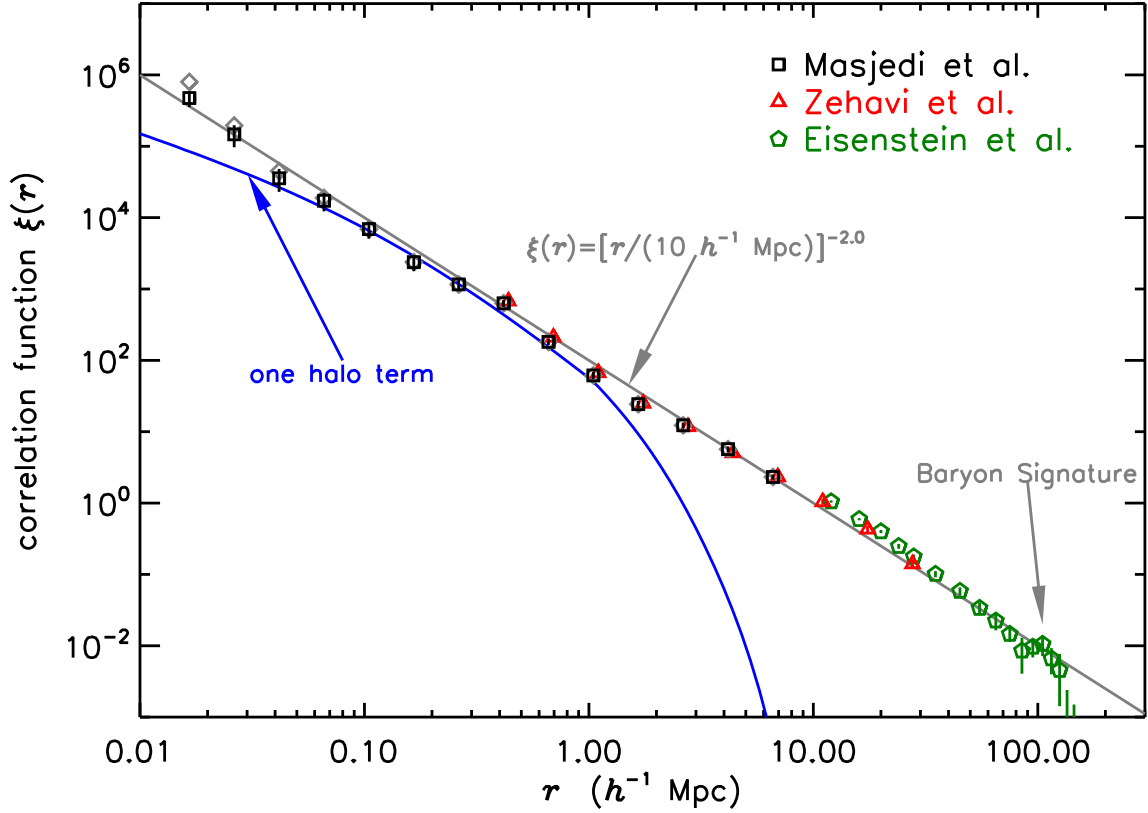


Fig. 4.— Real-space correlation function $\xi(r)$ for the LRG sample ($-23.2 < M_g < -21.2$ and $0.16 < z < 0.36$) calculated as described in the text on small scales, combined with real-space correlation function on intermediate scales from Zehavi et al. (2005a) and redshift-space correlation function $\xi(s)$ on large scales from Eisenstein et al. (2005) (data points from Zehavi results are shifted by 5% in the radial direction for illustration purposes). The gray diamonds show the result without photometric correction as in figure 1. The Blue line shows the 1-halo term of the correlation function calculated for the HOD parameters given by Zehavi et al. (2005b).

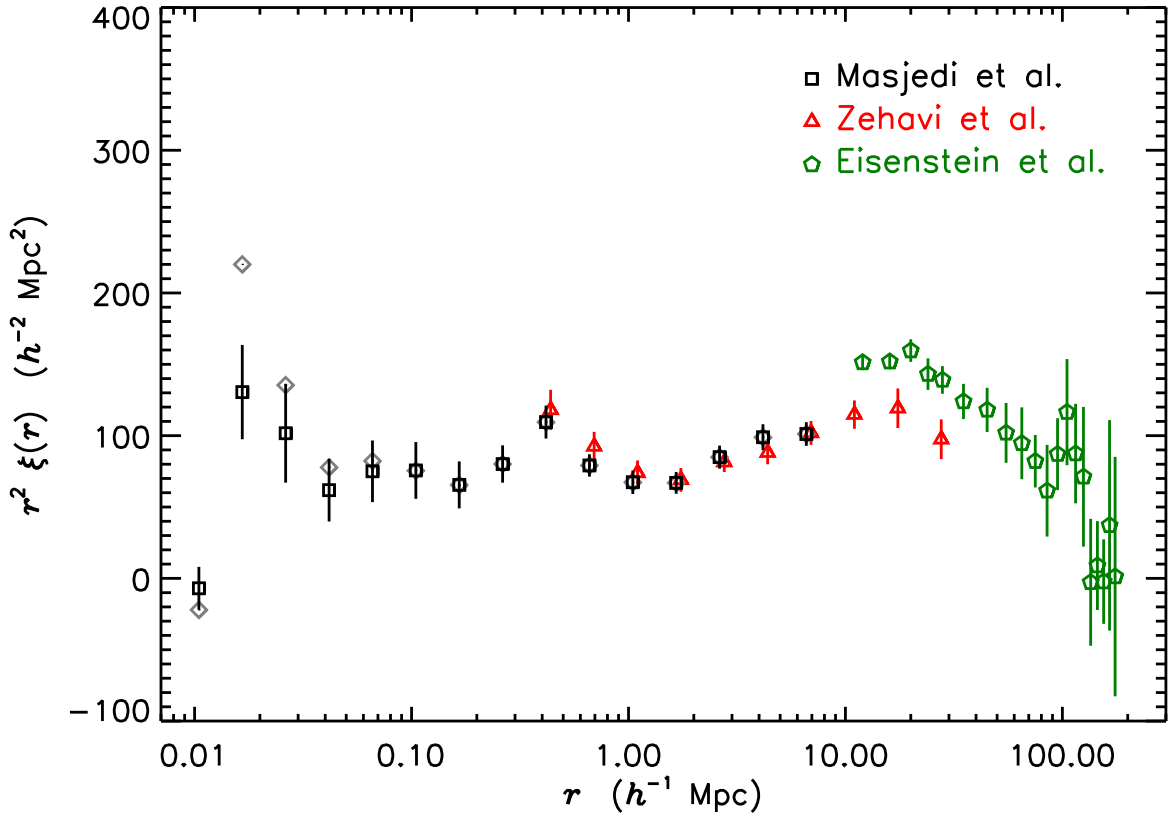


Fig. 5.— Same as Figure 4, but $\xi(r)$ divided by a r^{-2} power-law to accentuate the deviations from a power-law. Note that the difference between Zehavi et al. (2005a) and Eisenstein et al. (2005) is solely due to the difference between redshift space and real-space correlation functions.